First-Principles Determination of Electron-Ion Couplings in the Warm Dense Matter Regime

Jacopo Simoni* and Jérôme Daligault†
Theoretical Division, Los Alamos National Laboratory, Los Alamos, New Mexico 87545, USA

(Received 20 March 2019; revised manuscript received 12 April 2019; published 24 May 2019)

We present first-principles calculations of the rate of energy exchanges between electrons and ions in nonequilibrium warm dense plasmas, liquid metals, and hot solids, a fundamental property for which various models offer diverging predictions. To this end, a Kubo relation for the electron-ion coupling parameter is introduced, which includes self-consistently the quantum, thermal, nonlinear, and strong coupling effects that coexist in materials at the confluence of solids and plasmas. Most importantly, like other Kubo relations widely used for calculating electronic conductivities, the expression can be evaluated using quantum molecular dynamics simulations. Results are presented and compared to experimental and theoretical predictions for representative materials of various electronic complexity, including aluminum, copper, iron, and nickel.

DOI: 10.1103/PhysRevLett.122.205001

The last decade has seen remarkable progress in our ability to form and interrogate in the laboratory materials under conditions at the confluence of solids and hot plasmas in the so-called warm dense matter regime [1,2]. These experimental advances severely challenge our arsenal of theoretical techniques, simulation tools, and analytical models. In addition to including the coexisting quantum, thermal, disorder, and strong Coulomb interaction effects, theoretical approaches are needed that can also describe nonequilibrium conditions [3–14]. A particularly important property is the electron-ion coupling factor that measures the rate of energy exchanges between electrons and ions [5]. Indeed, experiments typically produce transient, nonequilibrium conditions and measurements may be misleading if recorded while the plasma species are still out of equilibrium. Moreover, like the electron-phonon coupling, the electron-ion coupling may be a unique indicator of the underlying electronic structure and of the basic interaction processes occurring in the warm dense matter regime. Remarkably, while even for simple materials various models offer diverging predictions (see Table I), the electron-ion coupling factor is now accessible to experimental measurements thanks to the diagnostic capabilities offered by the new generation of x-ray light sources [6–10].

Here, we use a combination of first-principles theory and *ab initio* molecular dynamics simulations to calculate the electron-ion coupling of materials under warm dense matter conditions. In the same way as with the now routine *ab initio* calculations of electrical and thermal conductivities [22–24], the approach offers a very useful comparison with the experimental measurements and a useful test of theories; it gives insight into the underlying physics, and it permits an extension into conditions not covered by the experiments. The electron-ion coupling is related to the friction coefficients felt by individual ions due to their nonadiabatic interactions with electrons. Each coefficient satisfies a Kubo relation given by the time integral of the autocorrelation function of the interaction force of an ion with the electrons, which is evaluated using density functional theory (DFT) based quantum molecular dynamics simulations. In this Letter, we outline the underlying theory and present results for a set of relevant materials and physical conditions. Details of mathematical proofs and algorithms will be presented in an extended manuscript [25]. Below, $\hbar$ is the reduced Planck constant and k_B is the Boltzmann constant.

We consider a material of volume V containing one atomic species. The material is described as a two-component system comprised of ions (mass $m_i = Am_u$, number density $n_i = N_i/V$, charge Ze) and of electrons (mass m_e, density $n_e = Zn_i$), where each ion consists of an atomic nucleus and its most tightly bound, unresponsive core electrons. We assume that the material can be described as an isolated, homogeneous, two-temperature system characterized at all times t by the temperatures $T_e(t)$

TABLE I. Electron-ion coupling for solid density aluminum at melting conditions.

Theoretical model	G_{ei} (10^{17} W/m^3 K)
Spitzer-Brysk	160 [15]
Fermi golden rule	5 [16,17]
Coupled modes	0.33 [18]; 0.1 [19]
Electron phonon	2.6 [20]; 5 [21]

and $T_i(t)$ of the electronic (e) and ionic (i) subsystems. Under the mild assumptions recalled below, the temperatures can be shown to evolve according to

$$c_i^0 \frac{dT_i}{dt} = G_{ei}(T_e - T_i), \qquad c_e \frac{dT_e}{dt} = -G_{ei}(T_e - T_i), \tag{1}$$

where $c_i^0 = 3n_i k_B/2$ is the kinetic contribution to the ionic heat capacity, c_e is the specific heat capacity of electrons at constant volume, and

$$G_{ei}(T_e, T_i) = 3n_i k_B \left\langle \frac{1}{3N_i} \sum_{I=1}^{N_i} \sum_{x=1}^{3} \gamma_{Ix,Ix}(\mathbf{R}, T_e) \right\rangle \tag{2}$$

is the electron-ion coupling, the focus of this work. It is given in terms of the thermally averaged friction felt by an ion as a result of its nonadiabatic interactions with electrons defined as follows.

Equations (1) and (2) result from a first-principles derivation under the following three assumptions [26,27]; (i) The dynamics of each ion can be described by that of the center $\mathbf{R}_I$ of its narrowly localized wave packet. This is justified here, since the thermal de Broglie wavelength $\Lambda = \hbar\sqrt{2\pi/m_i k_B T_i}$ ($\simeq 0.3/\sqrt{AT_i[\mathrm{eV}]}$ Bohr) of ions is generally much smaller than the spatial variations of forces acting on them due to their large mass and the relatively high temperatures. (ii) The typical ionic velocities are small compared to the typical electronic velocities. For instance, we assume $T_i/m_i \ll T_F/m_e$ or $T_i/m_i \ll T_e/m_e$ in the degenerate $T_e/T_F \ll 1$ or nondegenerate limit $T_e/T_F \gg 1$, respectively, where $T_F = (\hbar^2/2m_e k_B)(3\pi^2 n_e)^{2/3}$ [$\simeq 1.69(n_e[\mathrm{cm}^{-3}]/10^{22})^{2/3}$ eV] is the electronic Fermi temperature. This condition is generally respected due to the natural smallness of m_e/m_i, and is challenged only if $T_i \gg T_e$. (iii) Finally, we assume that there is a quasicontinuum of electronic states, as is the case for the metallic systems of interest here. Under these conditions, the ion dynamics follows the stochastic, Langevin-like equation

$$m_i \ddot{R}_{Ix} = F_{Ix}^{\mathrm{BO}} - m_i \sum_{J,y} \gamma_{Ix,Jy} \dot{R}_{Jy} + \xi_{Ix}.$$

Here F_{Ix}^{BO} is the adiabatic Born-Oppenheimer force felt by ion I along the x direction, which includes the interactions with other ions and with the instantaneous electrostatic potential of electrons. The other terms describe the effect of nonadiabatic transitions between closely spaced electronic states induced by the atomic motions and electronic excitations. These terms, which are not accounted for in current quantum molecular dynamics simulations, are responsible for the constant, nonreversible energy exchanges between electrons and ions. Like the buffeting of light liquid particles on a heavy Brownian particle, the nonadiabatic effects produce friction forces $m_i \sum_{J,y} \gamma_{Ix,Jy} \dot{R}_{Jy}$, and δ-correlated Gaussian random forces ξ_{Ix} with correlators $\prec \xi_{Ix}(t)\xi_{Jy}(t') \succ = 2m_e k_B T_e \gamma_{Ix,Jy} \delta(t - t')$. For a given ionic configuration $\mathbf{R} = (\mathbf{R}_1, \ldots, \mathbf{R}_{N_i})$, each friction coefficient is given by the Kubo relation

$$\gamma_{Ix,Jy}(\mathbf{R}, T_e) = \frac{1}{2m_i k_B T_e} \mathrm{Re} \int_0^\infty dt \langle \hat{\mathcal{F}}_{Ix}(t) \hat{\mathcal{F}}_{Jy}(0) \rangle_e \tag{3}$$

where $\langle \ldots \rangle_e$ is the electronic thermal average at temperature $T_e(t)$, and $\hat{\mathcal{F}}_{Ix}(t) = -e^{i\hat{H}_e t/\hbar}[\partial \hat{H}_e(\mathbf{R})/\partial R_{Ix}] e^{-i\hat{H}_e t/\hbar}$ is the electron-ion force operator at time t, where $\hat{H}_e(\mathbf{R}) = \sum_i (\hat{\mathbf{p}}_i^2/2m_e) + \sum_{i,I} v_{ie}(\hat{\mathbf{r}}_i - \mathbf{R}_I) + \sum_{i \neq j} (e^2/4\pi\epsilon_0) \times (1/|\hat{\mathbf{r}}_i - \hat{\mathbf{r}}_j|)$ is the electronic Hamiltonian. Here, for simplicity of exposition, the electron-ion interaction is described by a local pseudopotential $v_{ie}(r)$; in practice, this formalism allows us to deal with more elaborate descriptions [25] (e.g., the results shown below for noble and transition metals were obtained using plane-augmented wave pseudopotentials). The set of equations (1)–(3) is straightforwardly obtained by applying the Langevin-like dynamics to the evolution of the averaged ionic kinetic energy $\langle m_i \dot{\mathbf{R}}(t)^2/2 \rangle$, where $\langle \ldots \rangle$ denotes the average both over the Gaussian noise $\prec \ldots \succ$ and over a thermal ionic distribution at temperature $T_i(t)$ [25,26].

The expression (2) includes self-consistently the nonideal, quantum, and thermal effects that coexist in the warm dense matter regime. It reduces to well-known models in limiting cases [17], including the traditional Spitzer-Brysk formula in the hot plasma limit [15] and the Fermi golden rule formula in the limit of weak electron-ion interactions [16,17]. Moreover, it applies to hot solids with lattice temperature T_i much larger than the Debye temperature Θ_D (typically 0.01–0.04 eV [28]), where it extends the standard electron-phonon coupling $G_{e,ph}$ [29] by including ionic motions beyond the harmonic approximation.

By following techniques similar to those used for the *ab initio* calculation of electronic conductivities [23], we use the ionic and electronic structures calculated with standard quantum molecular dynamics simulations to evaluate the Kubo relations (3) needed in Eq. (2). Briefly, for each ionic configuration $\mathbf{R}$, the electronic structure is obtained from the solution of the Kohn-Sham equations $((\hat{\mathbf{p}}^2/2m_e) + V_{\mathrm{KS}}[\rho_e, \mathbf{R}])|\alpha\rangle = \epsilon_\alpha |\alpha\rangle$, where ϵ_α and $|\alpha\rangle$ are the single-particle Kohn-Sham energies and states, $\rho_e(\mathbf{r}) = \sum_\alpha n_\alpha |\langle \mathbf{r}|\alpha\rangle|^2$ is the electron density, and $n_\alpha = n(\epsilon_\alpha)$ with $n(\epsilon) = (1 + e^{-(\mu-\epsilon)/k_B T_e})^{-1}$ represents the Fermi-Dirac occupation number of the state α. In terms of the Kohn-Sham quantities, it can be shown that the coupling coefficients (3)

$$\gamma_{Ix,Jy} = -\frac{\pi}{m_i} {\sum_{\alpha,\beta}}' \frac{n_\alpha - n_\beta}{\epsilon_{\alpha\beta}} f_{Ix}^{\alpha\beta} f_{Jy}^{\beta\alpha} \delta(\epsilon_{\alpha\beta}/\hbar), \tag{4}$$

where the matrix elements $f_{Ix}^{\alpha\beta} = \langle\alpha|\hat{f}_{Ix}^{(sc)}|\beta\rangle$ and $\hat{f}_{Ix}^{(sc)}$ is the effective force along the x direction between ion I and a Kohn-Sham electron screened by other electrons.

Before showing results, we relate our approach to a model that has served as a reference in recent works,

$$G_{\text{e-ph}} \approx G_0^{\text{e-ph}} \int_{-\infty}^{\infty} \left(\frac{g(\epsilon)}{g(\epsilon_F)}\right)^2 \left(-\frac{\partial n(\epsilon)}{\partial \epsilon}\right) d\epsilon, \qquad (5)$$

which is a simplification in the high temperature limit [20,30] of the general electron-phonon coupling formula [29]. Here $g(\epsilon)$ is the electron density of states (DOS), which is computable with DFT, and $G_0^{\text{e-ph}} = \pi\hbar k_B \lambda \langle\omega^2\rangle g(\epsilon_F)$, where $\epsilon_F = k_B T_F$ is the Fermi energy, $\langle\omega^2\rangle$ is the second moment of the phonon spectrum, and λ is the electron-phonon mass enhancement factor. In previous works, the prefactor $G_0^{\text{e-ph}}$ was either set to match an experimental measurement at low electronic temperature [20] or was calculated *ab initio* [21,31,48]. Although derived for crystalline solids, the model (5) was used in recent works on warm dense matter systems [6–10]. Remarkably, an expression similar to Eq. (5) also results from Eq. (4) if one assumes that the matrix elements $f_{Ix}^{\alpha\beta}$ depend weakly on the energies, $f_{Ix}^{\alpha\beta} \approx f_{Ix}$, which yields

$$G_{ei} \approx G_0^{ei} \int_{-\infty}^{\infty} \left[\frac{g(\epsilon)}{g(\epsilon_F)}\right]^2 \left(-\frac{\partial n(\epsilon)}{\partial \epsilon}\right) d\epsilon, \qquad (6)$$

where $G_0^{ei} = |f_{Ix}|^2 g(\epsilon_F)^2$. The formulas (5) and (6) highlight the interplay between the DOS and the distribution of electronic states, which, as shown by Lin *et al.* [20], results in a strong dependence on the chemical composition and often on sharp variations with T_e. Below we compare our results to predictions based on (5) reported by others and on Eq. (6) with G_0^{ei} set to reproduce the value of G_{ei} at the lowest T_e considered. We find that the simplified models (5) and (6) tend to overestimate the dependence on T_e or predicts variations at odds with the full calculation.

Figures 1 and 2 (bottom panels) show results for $G_{ei}(T_e, T_i)$ for five representative materials and physical conditions, together with the predictions of previous models and with experimental data. Below we highlight some of the key findings. For each element, the upper panels show the electron density of states $g(\epsilon)$ and the Fermi-Dirac distribution function $n(\epsilon)$ at representative conditions. Our results were obtained with the open-source QUANTUMESPRESSO program [49]; the simulation details are given in the Supplemental Material [31]. In all cases, the material is prepared in the disordered, liquidlike state, except for aluminum for which we also show calculations in a finite-temperature fcc configuration.

Aluminum.—Figure 1(b) shows $G_{ei}(T_i, T_e)$ versus T_e at solid density $\rho = 2.7\ \text{g cm}^{-3}$ and $T_i = 0.1$ eV (slightly above the melting temperature 0.08 eV), together with other model predictions, including the Fermi golden rule

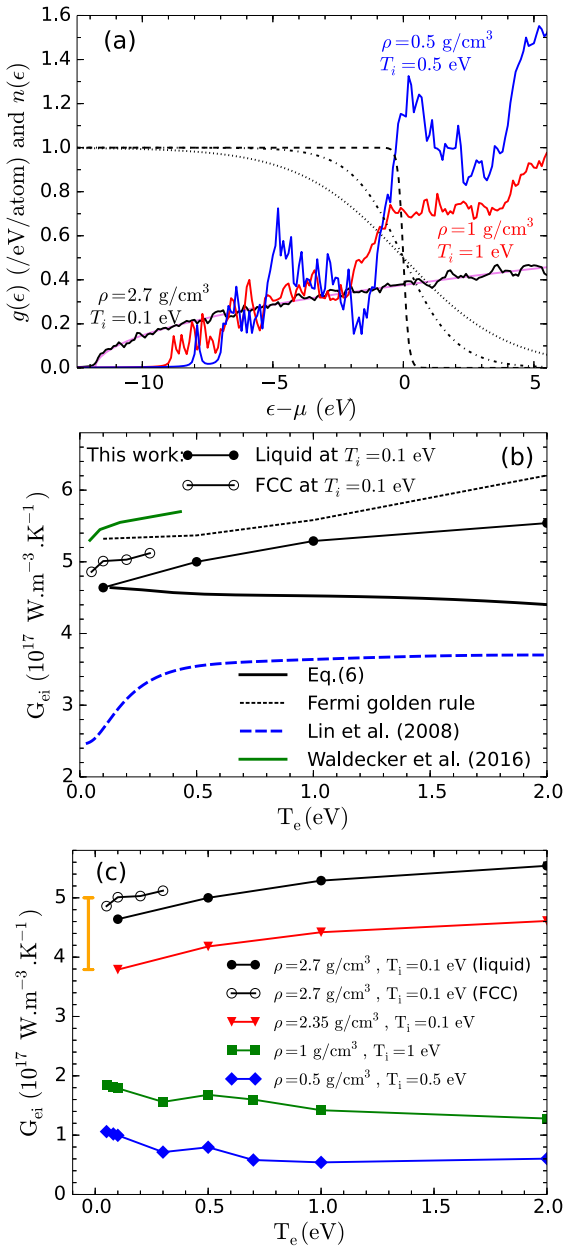

FIG. 1. (a) DOS of Al with $T_i = T_e$ and Fermi-Dirac distribution (dashed lines) for three electronic temperatures at $T_e = 0.1$, 1, 2 eV. Violet line is the DOS of the free-electron gas at 2.7 g cm^{-3}. Energy is measured with respect to the chemical potential $\mu(\rho, T_e)$. (b) $G_{ei}(T_e, T_i)$ vs T_e for solid density Al at $T_i = 0.1$ eV compared with other model predictions (see Table I). (c) $G_{ei}(T_e, T_i)$ vs T_e for Al at various densities and ionic temperatures. Vertical bar indicates the magnitude of the variation of G_{ei} at melting.

evaluated using the same pseudopotential v_{ie} of the *ab initio* calculations, and predictions based on Eq. (6) and the results of [20] and [21] based on Eq. (5) (see Table I for other predictions). G_{ei} steadily increases between 4.6 and 5.6×10^{17} W/Km^3 in the range $0.1 \le T_e \le 2$ eV, as a result of the growing number of excited electrons that

participate in the electron-ion scattering processes. Our results are in best agreement with the Fermi golden rule, which is expected given the free electronlike character of Al at solid density (see solid black and violet lines in Fig. 1). They differ from the prediction based on Eq. (6), which is similar to the result one obtains with the DOS of the free-electron gas at solid density [see Fig. 1(d) in [20]]. Figure 1(c) shows G_{ei} at other mass densities ρ and ionic temperatures T_i. As ρ decreases, the DOS shown in Fig. 1(a) progressively loses its free electronlike character. We find that the G_{ei} decreases with ρ at constant T_e, which is essentially an effect of the variation of the decreasing electron density [see n_e prefactor in Eq. (2)], and its variation with T_e changes from an overall increasing to a decreasing function of T_e. The figures also show calculations obtained for fcc lattices at solid density [open circles in Figs. 1(b) and 1(c)]. Our results are in good agreement with the result of Waldecker *et al.* [21] based on Eq. (5) with a DFT calculation of $G_0^{\text{e-ph}}$. At melting, the density is known to decrease from ~2.7 to ~2.35 $\mathrm{g\,cm^{-3}}$ [52] and G_{ie} decreases by about 25%, as indicated by the orange vertical bar in Fig. 1(c). This should be contrasted with the large change in the electrical resistivity at melting, which increases by a factor ~2.1 [52], in other words disorder has a higher effect on momentum relaxation than on energy relaxation.

Copper.—Warm dense copper has been the focus of several recent studies [7,9,20,48]. Figure 2(d) shows results at solid and melt densities, 8.96 and 8.02 $\mathrm{g\,cm^{-3}}$, and $T_i = 0.2$ eV (melting temperature is 0.117 eV), together with the measurements of [50] and [7]; the inset compares our result at 8.96 $\mathrm{g\,cm^{-3}}$ with Eq. (6) and with the results of [20] and [48] based on Eq. (5). We find that G_{ei} increases with T_e, with a faster variation above 0.5 eV when the d electrons, which are responsible for the prominent regions of high DOS in Fig. 2(a), can be excited and participate in the electron-ion energy exchanges. However, the variation is not as sharp and intense as that predicted using Eq. (5) of [20] and [48]. Unlike Ref. [20], we do not find a sharp increase of G_{ei} at small T_e, which was ascribed to the thermal excitations of d electrons. At solid density, we find $G_{ei} \simeq 2 \times 10^{17}$ $\mathrm{W/Km^3}$, in fair agreement with the old measurement 10^{17} $\mathrm{W/Km^3}$ of Elsayed-Ali *et al.* [50] for solid Cu. Our data lie slightly below the recent measurements reported in [7].

Iron.—Figure 2(e) shows the variation of G_{ei} with $T_e \leq 2$ eV for solid density Fe $\rho = 7.87$ $\mathrm{g\,cm^{-3}}$ at melting temperature $T_i = 0.156$ eV. We find that G_{ei} does not vary significantly over the temperature range considered, unlike the predictions based on Eqs. (5) [20] and (6).

Nickel.—Figure 2(f) shows the variation of G_{ei} with $T_e \leq 2$ eV for solid density Ni $\rho = 8.91$ $\mathrm{g\,cm^{-3}}$ at melting

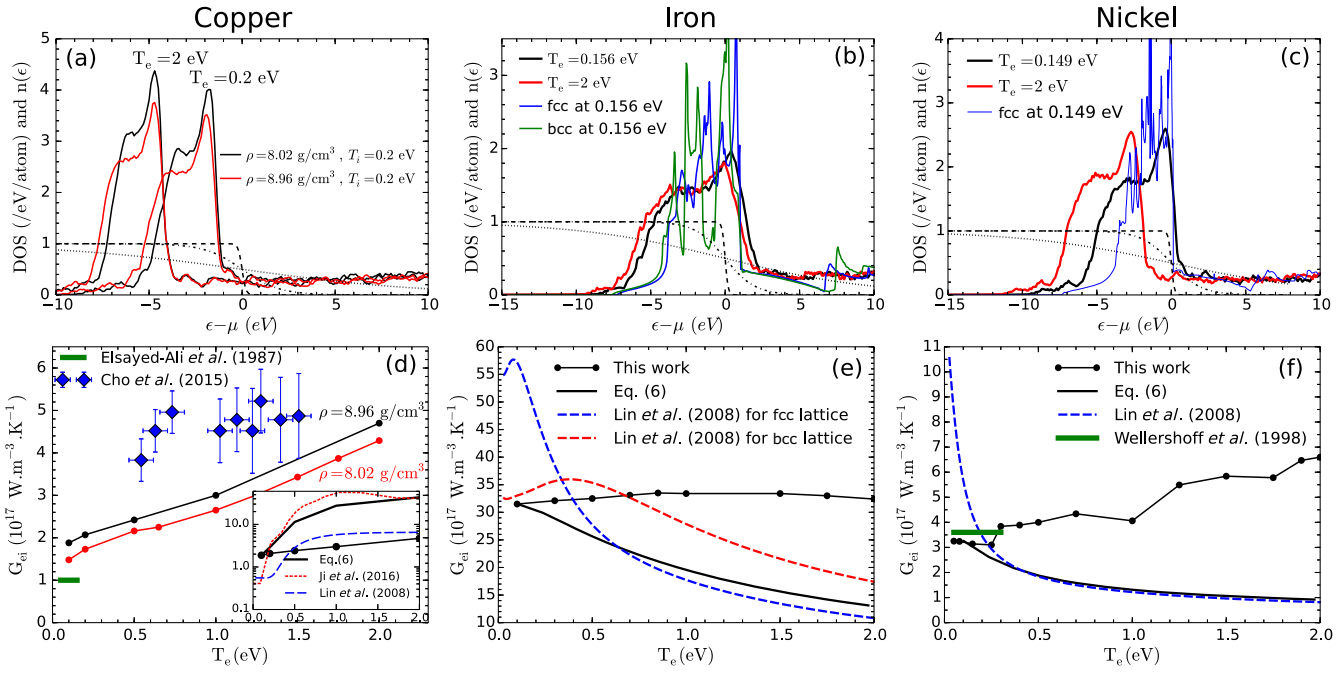

FIG. 2. op panels: same as Fig. 1(a) for Cu, Fe, and Ni at the conditions indicated in the legends. Bottom panels: $G(T_e, T_i)$ vs T_e for (d) solid and liquid density Cu at $T_i = 0.2$ eV, (e) solid density Fe at $T_i = 0.156$ eV, and (f) solid density Ni at $T_i = 0.149$ eV. In each case, the full lines with circles show the work's results, the full lines without symbols are obtained using Eq. (6) with G_0^{ei} set to reproduce the lowest T_e value, and the long dashed lines are the results based on Eq. (5) discussed in [20]. (d) Diamonds show the experimental results of [7]; bold green segment shows the measurement of [50] for solid Cu. Inset: dashed lines indicate model predictions based on Eq. (5) presented in [20,48]. (f) Bold green segment shows the measurement of [51].

temperature $T_i = 0.149$ eV. We find that G_{ei} increases from 3.1 to 5.6×10^{17} W/Km^3 over the temperature range, in contrast with the results based on Eq. (5) [20] and on Eq. (6). Our results at lower T_e are in good agreement with the measurement reported by Wellershoff *et al.* [51].

In summary, we have presented much-needed first-principles calculations of the electron-ion coupling factors of materials at the confluence of solids and plasmas based on a general expression in terms of the friction coefficients felt by ions due to the nonadiabatic electron-ion interactions. The approach serves as a useful comparison with the experimental measurements, permits an extension into conditions not covered by experiments, and provides insight into the underlying physics. We hope that this work will help assist and motivate future experiments and, ultimately, will help advance our understanding of the warm dense matter regime.

This work was supported by the U.S. Department of Energy through the Los Alamos National Laboratory through the LDRD Grant No. 20170490ER and the Center of Non-Linear Studies (CNLS). Los Alamos National Laboratory is operated by Triad National Security, LLC, for the National Nuclear Security Administration of U.S. Department of Energy (Contract No. 89233218CNA000001). The authors thank Dr. Dmitry Mozyrsky for helpful conversations.

*jsimoni@lanl.gov
†daligaul@lanl.gov

[1] *Frontiers and Challenges in Warm Dense Matter*, edited by F. Graziani, M. P. Desjarlais, R. Redmer, and S. B. Trickey, Lecture Notes in Computational Science and Engineering, Vol. 96 (Springer, New York, 2014).
[2] Plasma: At the Frontier of Scientific Discovery, U.S. Department of Energy Report of the Panel on Frontiers of Plasma Science, 2017, https://science.energy.gov/fes/community-resources/workshop-reports/.
[3] A. Ng, P. Celliers, G. Xu, and A. Forsman, Phys. Rev. E **52**, 4299 (1995).
[4] R. R. Fäustlin *et al.*, Phys. Rev. Lett. **104**, 125002 (2010).
[5] A. Ng, Int. J. Quantum Chem. **112**, 150 (2012).
[6] P. M. Leguay, A. Lévy, B. Chimier, F. Deneuville, D. Descamps, C. Fourment, C. Goyon, S. Hulin, S. Petit, O. Peyrusse, J. J. Santos, P. Combis, B. Holst, V. Recoules, P. Renaudin, L. Videau, and F. Dorchies, Phys. Rev. Lett. **111**, 245004 (2013).
[7] B. I. Cho, T. Ogitsu, K. Engelhorn, A. A. Correa, Y. Ping, J. W. Lee, L. J. Bae, D. Prendergast, R. W. Falcone, and P. A. Heimann, Sci. Rep. **6**, 18843 (2016).
[8] F. Dorchies and V. Recoules, Phys. Rep. **657**, 1 (2016).
[9] N. Jourdain, L. Lecherbourg, V. Recoules, P. Renaudin, and F. Dorchies, Phys. Rev. B **97**, 075148 (2018).
[10] T. Ogitsu, A. Fernandez-Pañella, S. Hamel, A. A. Correa, D. Prendergast, C. D. Pemmaraju, and Y. Ping, Phys. Rev. B **97**, 214203 (2018).
[11] J. Daligault and G. Dimonte, Phys. Rev. E **79**, 056403 (2009).
[12] Z. Chen, B. Holst, S. E. Kirkwood, V. Sametoglu, M. Reid, Y. Y. Tsui, V. Recoules, and A. Ng, Phys. Rev. Lett. **110**, 135001 (2013).
[13] J. Clérouin, G. Robert, P. Arnault, C. Ticknor, J. D. Kress, and L. A. Collins, Phys. Rev. E **91**, 011101(R) (2015).
[14] A. B. Zylstra, J. A. Frenje, P. E. Grabowski, C. K. Li, G. W. Collins, P. Fitzsimmons, S. Glenzer, F. Graziani, S. B. Hansen, S. X. Hu, M. G. Johnson, P. Keiter, H. Reynolds, J. R. Rygg, F. H. Séguin, and R. D. Petrasso, Phys. Rev. Lett. **114**, 215002 (2015).
[15] H. Brysk, P. M. Campbell, and P. Hammerling, Plasma Phys. **17**, 473 (1975).
[16] G. Hazak, Z. Zinamon, Y. Rosenfeld, and M. W. C. Dharma-wardana, Phys. Rev. E **64**, 066411 (2001).
[17] J. Daligault and D. Mozyrsky, High Energy Density Phys. **4**, 58 (2008).
[18] M. W. C. Dharma-wardana, Phys. Rev. E **64**, 035401(R) (2001).
[19] J. Vorberger and D. O. Gericke, AIP Conf. Proc. **1464**, 572 (2012).
[20] Z. Lin, L. V. Zhigilei, and V. Celli, Phys. Rev. B **77**, 075133 (2008); data available at http://www.faculty.virginia.edu/CompMat/electron-phonon-coupling/.
[21] L. Waldecker, R. Bertoni, R. Ernstorfer, and J. Vorberger, Phys. Rev. X **6**, 021003 (2016). See DFT line in Fig. (3c).
[22] M. P. Desjarlais, J. D. Kress, and L. A. Collins, Phys. Rev. E **66**, 025401(R) (2002).
[23] B. Holst, M. French, and R. Redmer, Phys. Rev. B **83**, 235120 (2011).
[24] T. Sjostrom and J. Daligault, Phys. Rev. E **92**, 063304 (2015).
[25] J. Simoni and J. Daligault (to be published).
[26] J. Daligault and D. Mozyrsky, Phys. Rev. E **75**, 026402 (2007).
[27] J. Daligault and D. Mozyrsky, Phys. Rev. B **98**, 205120 (2018).
[28] N. W. Ashcroft and N. D. Mermin, *Solid State Physics* (Harcourt College Publishers, London, 1976).
[29] P. B. Allen, Phys. Rev. Lett. **59**, 1460 (1987).
[30] X. Y. Wang, D. M. Riffe, Y.-S. Lee, and M. C. Downer, Phys. Rev. B **50**, 8016 (1994).
[31] See Supplemental Material at http://link.aps.org/supplemental/10.1103/PhysRevLett.122.205001, which includes Refs. [32–47], for the details of the quantum molecular dynamics simulations.
[32] P. Hohenberg and W. Kohn, Phys. Rev. **136**, B864 (1964).
[33] N. D. Mermin, Phys. Rev. **137**, A1441 (1965).
[34] W. Kohn and L. J. Sham, Phys. Rev. **140**, A1133 (1965).
[35] *Quantum Theory of the Electron Liquid*, edited by G. F. Giuliani and G. Vignale (Cambridge University Press, Cambridge, England, 2005).
[36] P. E. Blöchl, Phys. Rev. B **50**, 17953 (1994).
[37] P. Giannozzi *et al.*, J. Phys. Condens. Matter **21**, 395502 (2009).
[38] H. C. Andersen, J. Chem. Phys. **72**, 2384 (1980).

[39] V. Recoules, J. Clérouin, G. Zérah, P. M. Anglade, and S. Mazevet, Phys. Rev. Lett. **96**, 055503 (2006).
[40] A. Rousse, C. Rischel, S. Fourmaux, I. Uschmann, S. Sebban, G. Grillon, Ph. Balcou, E. Förster, J. P. Geindre, P. Audebert, J. C. Gauthier, and D. Hulin, Nature (London) **410**, 65 (2001).
[41] A. M. Lindenberg *et al.*, Science **308**, 392 (2005).
[42] M. Harb, R. Ernstorfer, C. T. Hebeisen, G. Sciaini, W. Peng, T. Dartigalongue, M. A. Eriksson, M. G. Lagally, S. G. Kruglik, and R. J. Dwayne Miller, Phys. Rev. Lett. **100**, 155504 (2008).
[43] B. J. Siwick, J. R. Dwyer, R. E. Jordan, and R. J. D. Miller, Science **302**, 1382 (2003).
[44] M. Kandyla, T. Shih, and E. Mazur, Phys. Rev. B **75**, 214107 (2007).
[45] R. Ernstorfer, M. Harb, C. T. Hebeisen, G. Sciaini, T. Dartigalongue, and R. J. D. Miller, Science **323**, 1033 (2009).
[46] J. P. Perdew and A. Zunger, Phys. Rev. B **23**, 5048 (1981).
[47] J. P. Perdew, K. Burke, and M. Ernzerhof, Phys. Rev. Lett. **77**, 3865 (1996).
[48] P. Ji and Y. Zhang, Phys. Lett. A **380**, 1551 (2016).
[49] P. Giannozzi *et al.*, J. Phys. Condens. Matter **29**, 465901 (2017).
[50] H. E. Elsayed-Ali, T. B. Norris, M. A. Pessot, and G. A. Mourou, Phys. Rev. Lett. **58**, 1212 (1987).
[51] S.-S. Wellershoff, J. Güdde, J. Hohlfeld, J. G. Müller, and E. Matthias, Proc. SPIE Int. Soc. Opt. Eng. **3343**, 378 (1998).
[52] M. Leitner, T. Leitner, A. Schmon, K. Aziz, and G. Pottlacher, Metall. Mater. Trans. A **48A**, 3036 (2017).